

Synthesis of Magnetic Polystyrene Nanoparticles Using Amphiphilic Ionic Liquid Stabilized RAFT Mediated Miniemulsion Polymerization

Sourav Chakraborty,^{†,‡} Klaus Jähnichen,[†] Hartmut Komber,[†] Ahmed A. Basfar,[§] and Brigitte Voit^{*,†,‡}

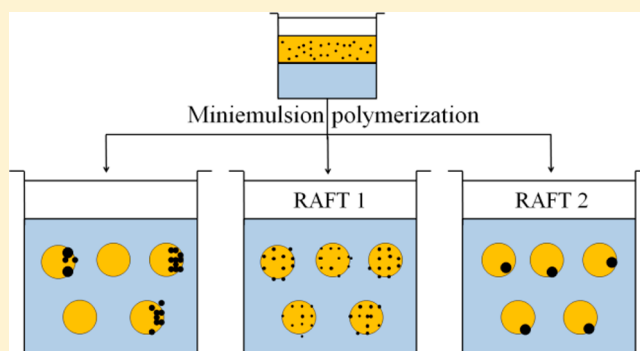
[†]Leibniz-Institut für Polymerforschung Dresden e.V., Hohe Straße 6, 01069 Dresden, Germany

[‡]Organic Chemistry of Polymers, Technische Universität Dresden, 01062 Dresden, Germany

[§]King Abdulaziz City for Science and Technology, P.O. Box 6086, Riyadh 11442, Saudi Arabia

Supporting Information

ABSTRACT: Imidazole based amphiphilic ionic liquids (ILs) were used as surfactants in miniemulsion polymerization (MEP) of styrene using a free radical process as well as reversible addition–fragmentation chain transfer (RAFT). Monodisperse polystyrene (PS) nanoparticles were obtained, demonstrating the efficiency of the amphiphilic IL as surfactant in MEP. IL stabilized miniemulsion was furthermore used to prepare polystyrene based magnetic nanoparticles (MNP). A large increase of the possible MNP content associated with very good colloidal stability was achieved using IL stabilized RAFT mediated MEP where a carboxyl functionalized chain transfer agent (CTA) was applied, allowing interaction with the MNP surface. The molecular weight and dispersity index of polystyrene, the content of MNP, and the morphologies of the hybrid nanoparticles were controlled by proper optimization of the concentration of initiator and CTA. The materials have been analyzed by NMR, GPC, DLS, SEM, TEM, and TGA. Finally, the magnetic properties of the materials were determined by vibrating sample magnetometer (VSM) analysis.



INTRODUCTION

Polymer magnetic composite (PMC) nanoparticles have raised a great deal of interest due to their potential use in several biomedical applications like magnetic resonance imaging,¹ nucleic acid purification,² enzyme immobilization,³ drug delivery,⁴ etc. The magnetic nanomaterials in the colloidal range have been successfully utilized in both therapeutic⁵ and diagnostic⁶ applications. The major challenge so far was the selection of suitable materials based on their various properties like particle size distribution, colloidal stability, content of MNP, presence of functionality, and most importantly toxicity. In the recent years, focus has also been turned on the synthesis of asymmetric polymer superparamagnetic composites for use as potential materials for applications in multimodal probes and biosensors.^{7,8} Besides the biomedical applications, there are several demands for PMC nanoparticles in the production of toner materials⁹ and also for the support and easy separation of catalyst in chemical reactions.¹⁰ The above facts necessitate a fruitful technique to produce PMC nanoparticles in dispersion or as solid materials. Several methods have been developed which include microfluidic-based synthesis,¹¹ selective surface modification,¹² and different kinds of heterogeneous polymerization.^{13,14} Among all these methods, miniemulsion polymerization (MEP) has been proven to be one of the most effective methods to prepare such materials. Regarding the synthesis of PMC nanoparticles using MEP, most of the work in the literature has proposed a single-step MEP process although no

more than 20 wt % of MNP with respect to the polymer could be encapsulated. Landfester et al.¹⁵ reported a strategy of multistep miniemulsion to encapsulate up to 40% MNP within the PS particles. Irrespective of the number of steps used for a successful encapsulation using MEP, several other parameters like nature of initiator, concentration of surfactant, and surface modifier of MNP are also quite important for deciding the characteristics of PMC nanoparticles. Surface modification of hydrophilic MNP (e.g., Fe₃O₄) is one of the essential requirements in this process. So different kinds of modifiers^{16–20} have been used to modify the hydrophilic surface of Fe₃O₄ into a hydrophobized one, with oleic acid (OA) being the most frequently used one. Besides the surface modifiers, initiator used for the polymerization also plays an important role to decide the location of MNP in the polymer particles. Kawaguchi et al.²¹ analyzed the effect of initiator concentration as well as its solubility on the morphological characteristics of PMC nanoparticles. A complete encapsulation of MNP was observed when water-soluble initiator was used while surface localization of MNP on the polymer particles was observed in the case of water-insoluble initiator. Recently, Elaissari et al.²² prepared anisotropic Janus magnetic polymer nanoparticles using styrene and acrylic acid as monomer and AIBN as sole

Received: April 16, 2014

Revised: June 12, 2014

initiator. The MNP were found to be accumulated on one side of the PS surface, thereby producing the Janus morphology. The influence of the concentration of surfactant has also been a matter of investigation in the encapsulation of MNP using MEP. Focarda et al.²⁰ reported the effect of surfactant concentration on the morphology of PMC nanoparticles. The distribution of MNP among the PS droplets was more homogeneous with reduction of the concentration of surfactant. In the absence of surfactant a core–shell morphology, with MNP as core and PS as shell material, was obtained with significant reduction in the formation of pure PS particles. The concentration of surfactant is indeed a very important parameter to avoid the formation of pure polymer nanoparticles resulting from homogeneous and micellar nucleation. A surfactant-free MEP of styrene using sodium *p*-styrenesulfonate (NaSS)²³ as self-stabilizing comonomer showed complete absence of secondary particles in the encapsulation of MNP by PS. So far most of the work was emphasized on using SDS as surfactant or on the surfactant-free MEP using NaSS, acrylic acid, or dextran as emulsion stabilizer.

Through the past two decades ILs have attracted a great deal of interest among the researchers due to its amazing properties like wide liquid range, excellent thermal stability, high ionic conductivity, low volatility, and ease of modification of its chemical structure. Among the different structural composition of ILs, amphiphilic ILs have become quite popular in the field of heterogeneous polymerization system. Biczók et al.²⁴ reported the ability of micelle formation of the alkyylimidazole based ILs in water. The critical micelle concentration (CMC) could also be varied by changing the type of alkyl chain or its length. This kind of surfactant-like behavior of alkyylimidazolium salts opened up the possibility of using such materials as stabilizer in different heterogeneous polymerization systems. Guerrero-Sanchez et al.²⁵ reported the suspension polymerization of styrene using ILs as stabilizer. Microemulsion polymerization was also conducted successfully using 1-*n*-dodecyl-3-methylimidazolium bromide as surfactant as reported by Yan and Texer.²⁶ In recent past, microwave-assisted emulsion polymerization has been performed using 1-*n*-dodecyl-3-methylimidazolium chloride as surfactant.²⁷ To the best of our knowledge, ILs have not been used as surfactant in MEP so far. In the present study, the influence of imidazole based amphiphilic ILs as surfactant in MEP and for the synthesis of PMC nanoparticles was investigated.

So far the major challenge in the preparation of PMC nanoparticles was to prepare high magnetic content materials using one-step MEP and also to avoid the formation of pure polymer particles. The loss of MNP during MEP due to insufficient encapsulation can only be reduced if the polymer droplets somehow attract the MNP through chemical or physical interaction. Inspired from the structural features of different surface modifiers used for MNP herein, it was aimed to synthesize a carboxyl functionalized polymer which was expected to keep the MNP attached to the polymer droplets. In the context of functional polymer synthesis, RAFT polymerization has become quite popular as different end functionality was possible to be achieved through the proper choice of CTA and its chemical conversion. In the field of MEP, RAFT polymerization was performed with some difficulties in colloidal stability and molecular weight distribution which were supposed to arise due to the superswelling effect caused by the presence of large amount of oligomers in the initial stage of polymerization.²⁸ Using nonionic surfactant instead of the

ionic one has been reported to have better control over the stability of RAFT mediated MEP.²⁹ However, a successful RAFT mediated MEP was reported recently by Zetterlund et al. using dioctyl sodium sulfosuccinate as an anionic surfactant which displayed good control and livingness together with good colloidal stability.³⁰

The objective of the present study is first to investigate the influence of amphiphilic IL as surfactant in free radical MEP as well as in RAFT mediated MEP and thereby to establish a fruitful environment for the synthesis of PMC nanoparticles. Finally, a detailed investigation of the characteristics of PMC nanoparticles along with the influence of RAFT mediated polymerization on their colloidal stability, morphology, composition, molecular weight distribution, and magnetic property will be performed.

EXPERIMENTAL SECTION

Materials and Characterization. 1-Methylimidazole, 1-bromohexadecane, 1-bromododecane, iron(II) chloride tetrahydrate, iron(III) chloride hexahydrate, oleic acid, 28–30% aqueous ammonia, carbon disulfide, and tetrabutylammonium hydrogen sulfate were all purchased from Aldrich and used as received. Sodium hydroxide (NaOH) pellets (Aldrich) were used to prepare 50% NaOH solution. Chloroform (Fischer Chemicals), acetone (Merck), concentrated hydrochloric acid (Merck), petroleum ether with boiling point 40–60 °C (Merck), hexadecane (Fluka), and AIBN (Fluka, 98%) were all used as received. Styrene was twice extracted with 0.1 N NaOH, followed by washing with water and brine in order to remove the stabilizer. Prior to use, it was heated over calcium hydride (Fluka) to 80 °C under vacuum until the evolution of hydrogen disappeared and distilled under vacuum. It was stored under nitrogen in a refrigerator.

The particle size measurements were performed with a Zetasizer NANO S (Malvern Instruments, UK) at a fixed scattering angle of 173°. The dynamic light scattering (DLS) measurements were performed in 0.01 N sodium chloride solution. 250 mg of the dispersion was weighed, and ca. 20 g of 0.01 N NaCl solution was added. The given values are the z_{average} (intensity based). The error of the measurements is about 5%.

The zeta potential of the as-synthesized PS latex was determined by means of electrophoretic mobility measurement, performed using a Zetasizer nano ZS (Malvern Instruments, UK). 50 mg of the as-synthesized PS latex was mixed with 20 g of 0.01 N NaCl solution. For the purpose of the present study to have information about surface charge of PS particles as well as their stability, only one sample was investigated at the original pH of the dispersion.

Gel permeation chromatography (GPC) measurements were performed with an apparatus of the Agilent Series 1100 (RI detection, 1PL_MIXED-B-LS-column [7.5 × 300 mm] and 10 mm PS gel Agilent column, chloroform 1.0 mL/min). PS was used as standard. This was the standard method for all of the samples. The samples containing MNP were filtrated to remove the MNP before the analysis.

Scanning electron microscopy (SEM) investigations were performed with an Ultra 55 plus (Zeiss). 250 mg of the latex was mixed with 20 g of water to prepare the samples. One drop was placed on a C-pad or a wafer. After air drying the samples were sputtered with 3 nm Pt.

Thermogravimetric analysis (TGA) was performed using a TGA Q5000 (TA Instruments). After 5 min isothermal at room temperature the temperature was increased up to 800 °C with 10 K/min under nitrogen.

Transmission electron microscope (TEM) analysis was performed by mixing ca. 50 mg of the dispersion with ca. 20 g of water. The sample specimen was prepared by taking 2 μL of the prepared solution on carbon coated TEM copper grid. After air drying the sample was investigated by TEM LIBRA 200 (Carl-Zeiss SMT, Oberkochen, Germany) working with acceleration voltage of 200 kV.

NMR spectra were recorded on an Advance III 500 NMR spectrometer (Bruker Biospin, Germany) operating at 500.13 MHz for ^1H and 125.77 MHz for ^{13}C . CDCl_3 was used as solvent, lock, and standard ($\delta(^1\text{H}) = 7.26$ ppm; $\delta(^{13}\text{C}) = 77.0$ ppm).

The magnetic properties of the materials were investigated using vibrating sample magnetometer (VSM) analysis. A Physical Property Measurement System (PPMS) (Quantum Design) was used which supplies 9 T field through a superconducting coil and operates with a vibrating sample magnetometer (Quantum Design) in the temperature range from 2 to 400 K. The dried sample was fixed in a closed container using a quick fix adhesive so that it cannot move inside the container. Then it was attached with the sample holder via an adaptor for the VSM measurement.

Experiments. *Synthesis of 2,2'-[Carbonthiobis(thio)]bis(2-methylpropionic acid) (CTA).* Synthesis of CTA was performed following the literature.³¹ Briefly, carbon disulfide (3.046 g), chloroform (11.938 g), acetone (5.808 g), tetrabutylammonium hydrogen sulfate (0.268 g), and 15 mL of petroleum benzene were mixed together in a double jacketed reactor which was cooled with tap water under an argon atmosphere. A thermometer was inserted into the reactor to observe the temperature of the reaction mixture. 50% aqueous NaOH (22.397 g) was added dropwise to the reaction mixture for 30 min (care has to be taken so that the temperature does not exceed 25 °C). After complete addition of sodium hydroxide solution, the reaction was carried out for 12 h. A yellow solid product was observed which was dissolved by the addition of 100 mL of water. Then the aqueous layer was acidified by 20 mL of concentrated HCl with stirring for 30 min under an argon atmosphere. The solid product thus obtained was filtered and washed with distilled water and then dried until constant weight. Figure 1 shows the chemical structure of

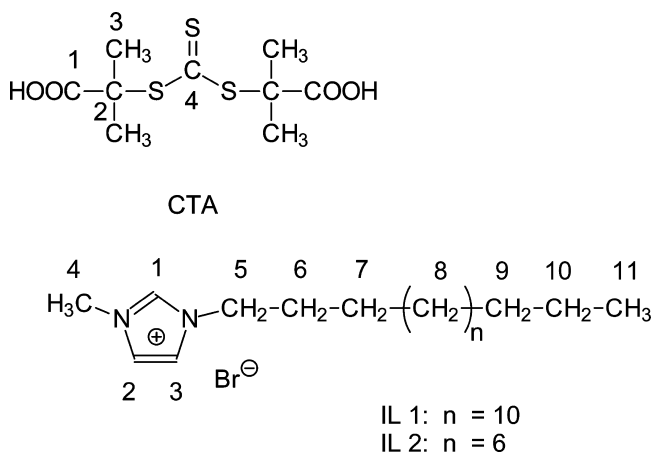


Figure 1. Structures of carboxyl functionalized CTA and surfactant ILs used in this study.

CTA. The ^1H and ^{13}C spectra of CTA are shown in Figure S11. NMR (CDCl_3): $\delta(^1\text{H})$ 1.71 ppm (s, H_3); $\delta(^{13}\text{C})$ 217.2 (C_4), 180.0 (C_1), 55.8 (C_2), 25.2 ppm (C_3); mp 172–175 °C.

Synthesis of Amphiphilic ILs. Synthesis of ILs was performed according to the method reported by Yao et al.³² Briefly, N-methylimidazole (0.125 mol) and 1-bromoalkane (0.15 mol) were added into a 250 mL three-necked round-bottomed flask. Isopropanol (20 mL) was added to reduce the viscosity. The mixture was stirred for 20 h under reflux at 70 °C. After removing isopropanol, the product was dissolved in 50 mL of water, and the excess materials were extracted 3 times with 25 mL of ethyl acetate each. The water was evaporated at 40 °C using a rotational evaporator. The product was then dried in a vacuum oven at 40 °C until constant weight. The structure of ILs is shown in Figure 1.

1-*n*-Hexadecyl-3-methylimidazolium bromide (IL 1); mp 62–65 °C; 1-*n*-dodecyl-3-methylimidazolium bromide (IL 2); mp 43–46 °C. NMR (CDCl_3): IL1: $\delta(^1\text{H})$ 10.32 (t, 1H, H_1), 7.55 (t, 1H, H_2), 7.38 (t, 1H, H_3), 4.28 (t, 2H, H_5), 4.10 (s, 3H, H_4), 1.88 (m, 2H, H_6), 1.4–

1.2 (26H, H_7 , H_9 , H_{10} , and $(\text{CH}_2)_{10}$), 0.84 ppm (t, 3H, H_{11}); $\delta(^{13}\text{C})$ 137.62 (C_1), 123.41 (C_2), 121.67 (C_3), 50.17 (C_5), 36.74 (C_4), 31.84 (C_9), 30.24 (C_6), 29.7–28.9 (CH_2)₁₀, 26.71 (C_7), 22.60 (C_{10}), 14.03 ppm (C_{11}). IL2: $\delta(^1\text{H})$ 10.31 (t, 1H, H_1), 7.52 (t, 1H, H_2), 7.37 (t, 1H, H_3), 4.29 (t, 2H, H_5), 4.10 (s, 3H, H_4), 1.88 (m, 2H, H_6), 1.4–1.2 (18H, H_7 , H_9 , H_{10} , and $(\text{CH}_2)_6$), 0.84 ppm (t, 3H, H_{11}); $\delta(^{13}\text{C})$ 137.48 (C_1), 123.49 (C_2), 121.73 (C_3), 50.13 (C_5), 36.72 (C_4), 31.80 (C_9), 30.22 (C_6), 29.5–28.8 (CH_2)₆, 26.19 (C_7), 22.57 (C_{10}), 14.00 ppm (C_{11}).

The ^1H and ^{13}C NMR spectra of both ILs are shown in Figure S12.

Synthesis of Oleic Acid Coated MNP Using the Coprecipitation Method. OA coated MNP were synthesized according to the coprecipitation method followed by Focarda et al.²⁰ with a little modification. Briefly, 10.8 g of $\text{FeCl}_3 \cdot 6\text{H}_2\text{O}$ and 3.9 g of $\text{FeCl}_2 \cdot 4\text{H}_2\text{O}$ were dissolved in 200 mL of deionized water. Then 3.5 g of OA was dissolved in 120 mL of acetone, and the above two solutions were mixed under stirring using a mechanical stirrer at 500 rpm under an argon atmosphere. After 30 min, 25 mL of 28–30 wt % NH_4OH solution was added over a period of 10–15 min. The resulting suspension was stirred for 1 h at room temperature and then heated at 85 °C for 1 h more. Temperature was raised to 110 °C and kept for 1 h more to remove excess ammonia. Then it was cooled to room temperature. The black particles were separated using a magnet from outside, and the supernatant liquid was decanted. The particles were washed several times with distilled water until the washed liquid comes to the pH range ~7–8. Then the particles were washed with methanol to remove excess OA, which is not adsorbed onto the surface of MNP. Finally the particles were dried in vacuum oven at 50 °C until constant weight.

Miniemulsion Polymerization Using IL as Surfactant. The aqueous phase was prepared first by dissolving IL in water. Then the organic phase was prepared by mixing purified styrene, hexadecane, AIBN, and RAFT agent (in the case of RAFT mediated MEP) until the solid particle dissolves. Both the phases were mixed, and the mixture was degassed 5 times using the Ar/vacuum cycle. Then the mixture was stirred at 600 rpm using a glass stirrer under an argon atmosphere for 1 h to prepare the pre-emulsion. Then the miniemulsion was prepared by sonication of the pre-emulsion for 10 min (duty cycle 90%) with an ultrasonic disintegrator Branson 450 W using a 1/2 in. minitip under inert atmosphere. During the sonication a cooling of the reaction vessel by ice water was performed in order to avoid a heating of the mixture. Finally, the prepared miniemulsion was polymerized at 70 °C under an Ar atmosphere using a mechanical stirring at 400 rpm. The detailed recipe is shown in Table 1.

Synthesis of PMC Nanoparticles Using IL Stabilized Miniemulsion. The organic phase was prepared by mixing styrene, hexadecane, OA coated MNP, and CTA (in the case of RAFT mediated MEP) followed by sonication for 1 min in an ultrasound bath at room temperature. AIBN was added after sonication. The aqueous phase was prepared by mixing IL with water and mixed with organic phase. After mixing, the procedure described previously was repeated using the recipe described in Table 1.

Removal of Coagulum (If Any). After the polymerization, the formed dispersion was poured through a mesh (pore size 20 μm) and then used for the analytical investigations. Finally, the rest in the mesh and the rests from the stirrer and the vessel were transferred into a frit using water. The coagulum was washed with water and dried in a vacuum at room temperature in order to determine the quantity of coagulum.

Isolation of Solid Particles for Characterization. About 2 g of the final dispersion was weighed in a Petri dish and kept overnight at room temperature. The air-dried products were further dried in a vacuum at room temperature until the weight was constant, and then the solid content was calculated. P_4O_{10} was used as drying agent in the vacuum oven. The dried product was used for characterization.

Calculation of Monomer Conversion. The conversion of monomer was determined by the gravimetric method considering the solid content of the dispersion. In the case of PMC nanoparticles, considering the contribution of MNP in solid content of the

Table 1. Experimental Details for the Synthesis^a of PS and PMC Nanoparticles

sample	MNP ^b (wt %)	AIBN (g)	CTA (g)	IL1 (g)	IL2 (g)	react time (h)
PS 1 ^c		0.130		0.10		6
PS 2 ^c		0.130			0.09	6
PS 3		0.022	0.076	0.10		14
PS 4		0.022	0.113	0.10		14
PS 5		0.022	0.076		0.09	14
PMC 1	4	0.130		0.10		8
PMC 2	8	0.130		0.10		8
PMC 3	12	0.130		0.10		8
PMC 4	8	0.130			0.09	8
PMC 5	8	0.022	0.038	0.10		14
PMC 6 ^d	8	0.022	0.076	0.10		14
PMC 7	8	0.022	0.150	0.10		14
PMC 8	8	0.130	0.076	0.10		20
PMC 9	8	0.130	0.076		0.09	20

^a7.98 g of styrene, 36.0 g of water, and 0.575 g of hexadecane were used in all cases. The sonication time and polymerization temperature were fixed to 10 min and 70 °C, respectively (exceptions PS 1 and PS 2). ^bWith respect to monomer. ^cA series of investigations were performed using this recipe to investigate the influence of the concentration of surfactant and sonication time duration on particle size of PS. ^dPolymerization was continued up to 40 h to investigate the influence of monomer conversion on the final MNP content of the material.

dispersion, we have calculated the conversion of monomer using the equation

$$\% \text{ conversion} = \frac{S - M - V}{L \times W} \times 100\%$$

where *S* represents the weight of dried sample, *M* is the theoretical weight of MNP in the dried sample, *V* represents the theoretical weight of the nonvolatile, chemically nonreactive component of the recipe in the dried sample, *L* is the weight of the latex taken for determination of monomer conversion, and *W* is the weight fraction of monomer in the recipe.

RESULTS AND DISCUSSION

Synthesis of Oleic Acid Coated MNP. In order to disperse MNP in styrene, hydrophobization of the surface of

MNP by OA was performed using the coprecipitation method.²⁰ The content of OA on the MNP surface was investigated by TGA analysis, as shown in Figure 2a. Considering the residue in the TGA curve as the weight fraction of the inorganic substance (here MNP), the content of OA was estimated to be about 22 wt %. The weight loss curve of pure OA showed a *T*_{max} of 272 °C. In the TGA curve of OA modified MNP two ranges of weight loss were found. The small weight loss in the first range between 166 and 266 °C might reflect the liberation of residual free OA with a *T*_{max1} at 211 °C, whereas a significant weight loss in the second range between 290 and 440 °C with a *T*_{max} at 333 °C was observed which is possibly due to the liberation/decomposition of OA attached to the surface of MNP. The magnetization curve of OA coated MNP is shown in Figure 2b. The saturation magnetization was observed to be 53 emu/g.

The hydrophobization of the surface was confirmed by a comparative MNP dispersion analysis between water and toluene as medium (Figure SI 3a). The MNP were easily dispersed in toluene just by manual shaking whereas in water it was not possible to disperse even with the help of sonication. The morphology of the MNP was analyzed by TEM using the MNP dispersed in toluene. The particle size was mostly around 10–20 nm. A relatively broad distribution of particle size was observed, which has to be expected in the case of the coprecipitation method. The MNP were observed to appear as aggregates of dark spheres up to 28–42 nm surrounded by the attached OA layer appearing gray. The TEM image of OA coated MNP is shown in (Figure SI 3b).

Miniemulsion Polymerization Using Amphiphilic ILs as Surfactant. The surfactant behavior of amphiphilic ILs has not been explored in the field of miniemulsion so far. So we aimed to establish an IL stabilized miniemulsion process which can produce monodisperse polymer nanoparticles based on polystyrene. From the chemical structure of amphiphilic ILs used in this study, 1-*n*-hexadecyl-3-methylimidazolium bromide (IL 1) and 1-*n*-dodecyl-3-methylimidazolium bromide (IL 2) (Figure 1), they were expected to behave like a cationic surfactant, and thus the PS particles should have a positive charge on their surface. Zeta potential determination of PS latex at the original pH (6.4) of the latex confirmed the presence of positive charge on the surface of PS particles. On the other

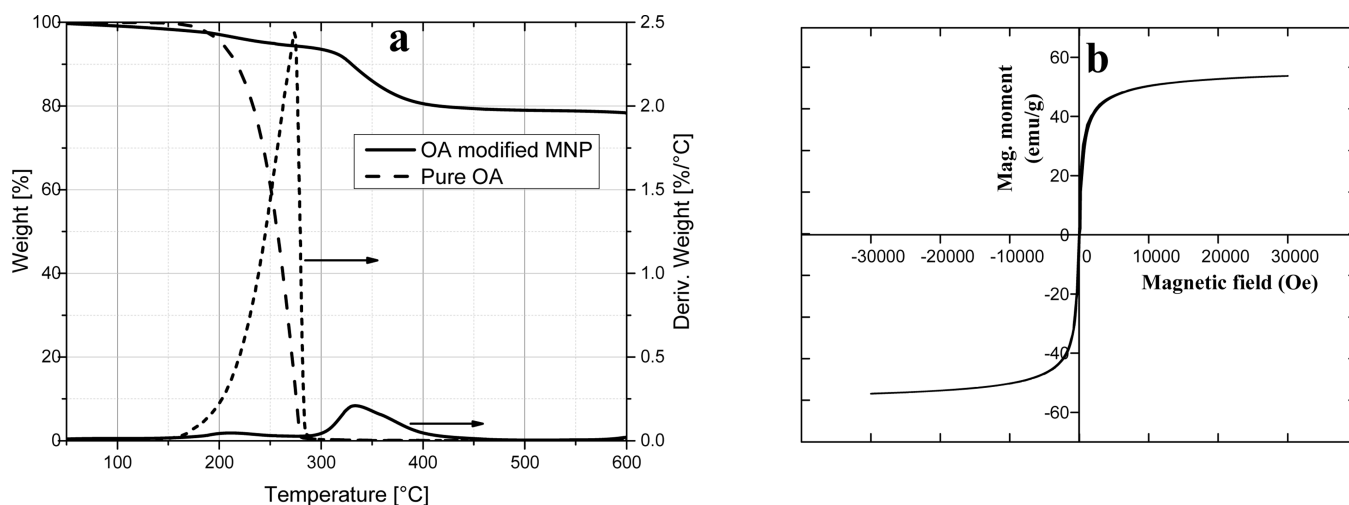


Figure 2. Thermal and magnetic properties of OA modified MNP: (a) TGA curve of pure OA and OA modified MNP and (b) magnetization curve of OA modified MNP.

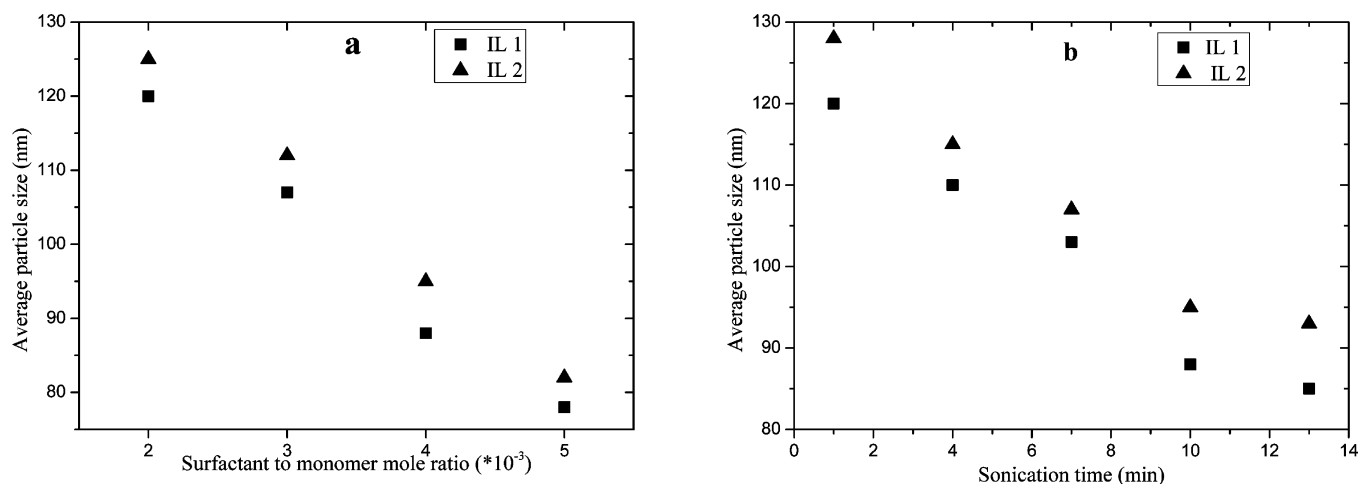


Figure 3. Dependence of particle size on the recipe and the sonication conditions: (a) influence of surfactant to monomer molar ratio on average particle size and (b) influence of sonication time during miniemulsion on average particle size. In both cases (a) and (b), recipe was followed as given for PS 1 and PS 2 in Table 1.

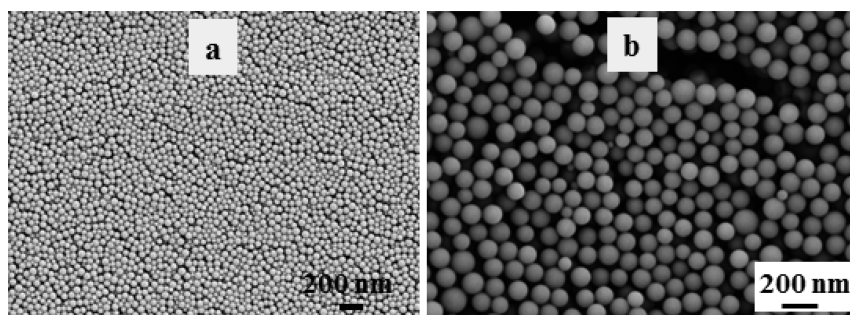


Figure 4. SEM image of PS particles synthesized by (a) IL 1 (PS 1) and (b) IL 2 (PS 2) stabilized MEP. Sonication time was performed for 10 min in both cases.

hand, the value of zeta potential (54 ± 0.8 mV) also indicated a high stability of the PS latex. The influence of IL concentration on the particle size (DLS) was observed to follow a similar kind of behavior to that of a conventional anionic surfactant like SDS as well as of cetyltrimethylammonium bromide (CTAB) as an example for a cationic surfactant used in MEP. In the Supporting Information, experimental details and results of IL, SDS, and CTBA stabilized MEP under identical conditions are presented, proving that ILs are as effective as surfactants in MEP as SDS and even more effective in stabilizing and controlling the size of polymer particles in MEP than CTAB (see Supporting Information, Figures SI 8 and SI 9). The particles size shows in all cases a tendency to decrease with increasing the amount of surfactant. In an ideal scenario for MEP, the concentration of surfactant should be below the CMC. In the present system, the surfactant IL 1 has a very low CMC (0.61 mM),²⁴ and therefore, it had to be used in MEP at a concentration higher than its CMC, since it was impossible to produce a stable miniemulsion at a concentration below its CMC value. In order to reduce the chance for micellar nucleation as much as possible, we used another imidazole based IL surfactant with a dodecyl hydrocarbon chain, 1-dodecyl-3-methyl imidazolium bromide (IL 2), which has a CMC value of 9.8 mM,²⁴ much higher than that of IL 1. Thus, a stable MEP was possible to conduct at a much lower concentration of IL2 compared to its CMC. A comparative study between two surfactants regarding the influence of surfactant concentration on particle size of PS latex was

performed and is shown in Figure 3a. The pattern of the curves did not show any dissimilarity between two ILs; moreover, the average particle size and dispersion index value were quite close in both cases. It indicates that the occurrence of micellar nucleation in the case of IL 1 stabilized MEP was almost negligible; otherwise, it would produce a much broader distribution in the particle size analysis. In the miniemulsion system the creation of droplets as well as their size can be influenced on changing the sonication time, and thereby we investigated the influence of sonication time on particle size distribution of the PS latex. A gradual decrease in the average particle size was observed in both systems with increasing sonication time, as shown in Figure 3b. Antonietti et al. reported a similar kind of behavior with other surfactants.³³ This also indicates the predominant droplet nucleation in both the systems. The particle size became nearly constant after 10 min of US for both the cases which is attributed to the lowest particle size that was possible to achieve using the mentioned recipe and conditions.

The morphology of PS particles was investigated using SEM (Figure 4). Monodisperse particles were observed in both systems with an average diameter of 120 nm down to 80 nm, depending on the surfactant concentration and sonication time. In some cases, very few particles in the order of 300 – 400 nm were observed. But considering the low fraction of such big particles, it is almost negligible compared to the dominating fraction of smaller PS particles.

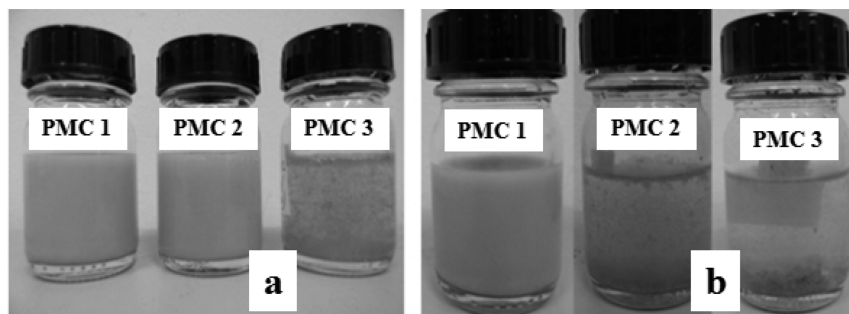


Figure 5. Stability of latexes after dilution (a) immediately and (b) 3 days after polymerization.

Synthesis of PMC Nanoparticles Using IL Stabilized MEP. For the preparation of PMC nanoparticles, at first, three experiments were performed with IL 1 as surfactant using different amounts of feed MNP content. The colloidal stability was observed by keeping the diluted latex for long duration. The dilution was made at the same concentration as for the DLS study (without addition of electrolyte). Figure 5 indicates a gradual decrease in the stability of dispersion with increasing amount of feed MNP. The experiment with 12 wt % feed MNP (PMC 3) showed very poor stability that was indicated by an immediate precipitation of the PMC nanoparticles from the dispersion (magnetism of the particles was confirmed by attraction toward an external magnet, as shown in Figure 6a).

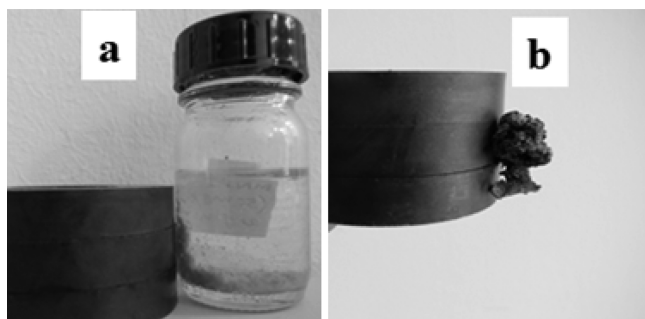


Figure 6. Magnetism of the nanoparticles from PMC 3 proved by the attraction toward external magnet (a) and presence of MNP in the coagulum from PMC 3 proved by the attraction toward external magnet (b).

The sample with 8 wt % feed MNP (PMC 2) showed a reasonable stability where the precipitation started only after keeping the dispersion standing for nearly 3 days. The least MNP content dispersion (PMC 1 with 4 wt % feed MNP) was observed to be a very stable throughout an observation time of even 3 weeks. The particle size distribution was investigated using DLS analysis (Table 2) which shows an increase in the average particle size as well as the dispersion index with increasing the feed MNP content from 4 to 8 wt %. Because of

the immediate precipitation of PMC nanoparticles in the case of sample PMC 3, DLS could not be performed.

In order to check the dispersion scenario using IL 2 as surfactant, an experiment (PMC 4) with 8 wt % feed MNP content was performed which showed similar latex stability as that of PMC 2. The DLS analysis (Table 2) also displayed very similar results regarding the particle size distribution. Thus, one can assume again that there is no high influence from the micellar nucleation in the case of IL 1 stabilized MEP; otherwise that would result in broader particle size distribution.

Apart from the instability in the dispersion of PMC 3, the polymerization eventually ended up producing a high amount of coagulum (~35%). The final MNP content of PMC nanoparticles was investigated using TGA. The results are summarized in Table 2.

In the case of PMC 1, the final MNP content fitted reasonably well with the feed MNP content. Considering the monomer conversion of 95% along with 5 wt % coagulum the reduction of ca. 0.8 wt % MNP content in the final composite material was satisfactory. But with increasing the feed MNP to 8 wt % (PMC 2), the reduction of MNP content in the particles became higher up to 2.5 wt %, which was quite a significant loss. The loss of MNP became even more pronounced with increasing the amount of feed MNP to 12 wt % (PMC 3). This can be correlated with an increased amount of coagulum with increase in feed MNP content as reported in Table 2. In order to know the nature of coagulum, we performed a TGA investigation of the coagulum from PMC 3 which suggested that a hybrid material (containing both organic and inorganic materials) made up the coagulum. The coagulum showed attraction toward an external magnet which confirmed the presence of MNP within it (Figure 6b). Altering the surfactant from IL1 to IL2 keeping the molar surfactant concentration constant, thereby using IL2 below its CMC did not improve the stability of the dispersion as well as the final content of MNP (compare PMC 2 to PCM 4, Table 2). We assume that inefficient interactions between the PS matrix and OA coated MNP or the inability to hold the MNP inside or on the surface of PS spheres due to phase segregation is

Table 2. Characterization Results for PMC Nanoparticles Synthesized by IL Stabilized MEP

sample	feed MNP ^a (wt %)	av particle size (nm) [dispersion index]	coagulum (wt %)	solid content (wt %)	conversion of monomer (%)	MNP content from TGA (wt %)
PMC 1	4	122 [0.03]	5	19	96	3.2
PMC 2	8	136 [0.07]	8	18	90	5.5
PMC 3	12	n.d.	35	17	80	8.2
PMC 4 ^b	8	143 [0.06]	7	18	90	5.8

^aWith respect to monomer. ^bIn the case of PMC 4, IL 2 was used as surfactant. In all other cases, IL 1 was used as surfactant.

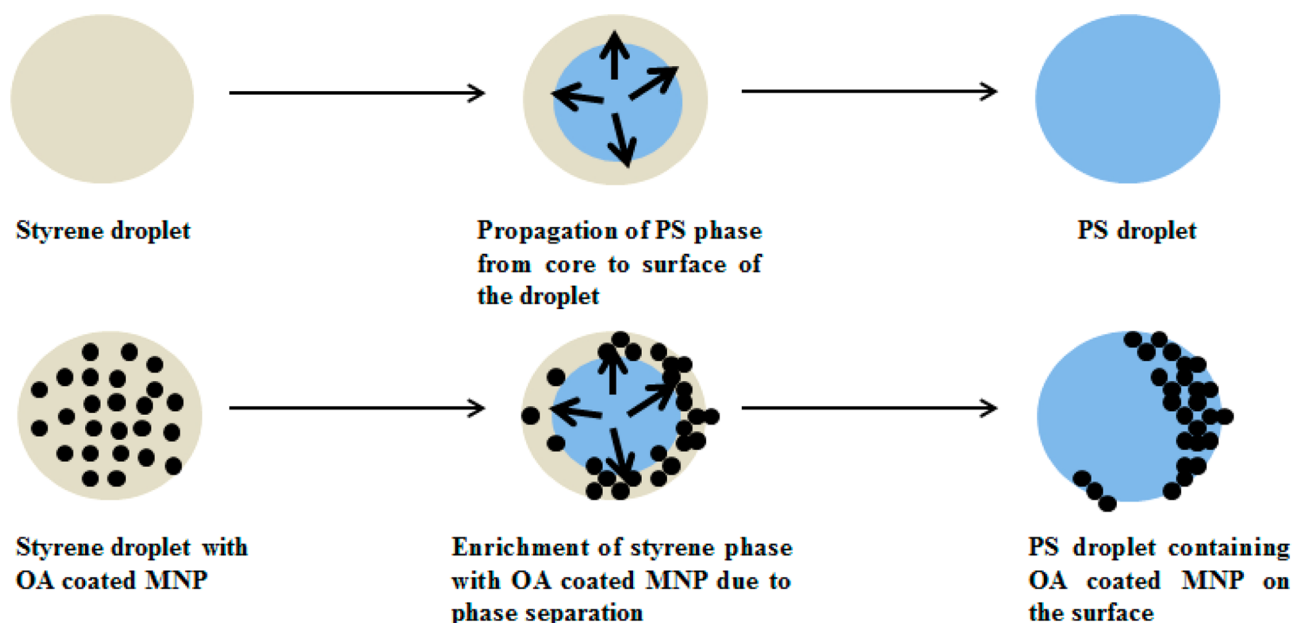


Figure 7. Schematic representation of the enrichment of styrene phase with OA-coated MNP as a result of phase separation between MNP and developing PS phase in the AIBN initiated MEP.

Table 3. Characterization Results from IL Stabilized Non-RAFT and RAFT Mediated MEP

sample	AIBN (g)	CTA (g)	AIBN:CTA (mole ratio)	av particle size (nm) [dispersion index]	M_n (g/mol)	dispersity index \bar{D}	solid content (wt %)	conv (%)
PS 1 ^a	0.130			93 [0.03]	2.61×10^6	2.0	18	100
PS 2 ^b	0.130			103 [0.05]	2.43×10^6	2.2	18	100
PS 3 ^a	0.022	0.076	1:2	125 [0.05]	18000	1.7	16	84
PS 4 ^a	0.022	0.113	1:3	140 [0.07]	12000	1.6	13	70
PS 5 ^b	0.022	0.076	1:2	133 [0.04]	19000	1.8	16	82

^aIL 1 as surfactant. ^bIL 2 as surfactant.

responsible for the low MNP content in the latex compared to the feed. Elaissari et al.²² also found a similar scenario in the SDS stabilized MEP for the synthesis of anisotropic magnetic polymer particles where a final MNP content of only 19 wt % was possible to achieve using 30 wt % of feed MNP, indicating a significant loss of MNP through the formation of coagulum.

The amount of feed MNP also had a measurable influence on the monomer conversion which became lower as the amount of MNP increased. With increase in the amount of feed MNP from 4 to 12 wt %, the conversion of monomer goes down from 95% to 80% (Table 2). The reduction in monomer conversion in the presence of MNP has also been reported in the literature.^{15,22} Involvement of OA in the polymerization¹⁵ might be a reason for such reduction in conversion, leading to consumption of initiator, although increasing the amount of AIBN did not increase the monomer conversion. It can be assumed that the influence of MNP may arise from their preferred location in the styrene monomer phase within the droplet due to their immiscibility with the final PS phase as shown in Figure 7.

Synthesis of PMC Nanoparticles Using RAFT Mediated MEP. In order to overcome the problem of inhomogeneity in the distribution of MNP among the PS particles as well as the loss of MNP content in the composite materials, RAFT mediated MEP was performed to synthesize the PMC nanoparticles. Considering the affinity of carboxylic acid group toward the surface of MNP, we choose a carboxylic acid terminated CTA (Figure 1) expecting the carboxyl group

and the trithiocarbonyl moiety of CTA would enhance the interaction of the PS chain with MNP; consequently, the distribution of MNP among the PS droplets would be more homogeneous. At first, the RAFT mediated MEP was conducted in the absence of MNP in order to investigate the morphology of the RAFT polymerized PS particles and the terminal functionalization of the PS chain. Two experiments were performed using IL1 as surfactant to observe the influence of concentration of CTA in the molecular weight development and dispersity index. In addition to that, one IL2 stabilized RAFT mediated MEP was also performed. Table 3 represents the GPC investigation of PS synthesized by different non-RAFT and RAFT mediated MEP. Irrespective of the nature of IL, a large reduction in the molecular weight value M_n was observed in the presence of CTA as compared to the non-RAFT MEP. The reduction of M_n could be controlled by tuning the AIBN to CTA mole ratio and the dispersity index \bar{D} in all RAFT mediated MEP was with 1.5–1.9 significantly lower as in the free radical process, both indicating an effective chain transfer, even though \bar{D} was not as low as for a typical bulk RAFT polymerization.³¹ The purpose of the present study was to successfully attach the terminal carboxylic group to the PS chain via RAFT mediated MEP. The confirmation of the presence of terminal carboxyl group in PS chain was not possible by any spectroscopic analysis due to the still high molecular weight. Hence, a model reaction via bulk RAFT polymerization was performed with the same CTA, which produced low molecular weight PS, to confirm the attachment

of terminal carboxylic group at the PS chain ends. Figure 8 depicts the ^1H NMR spectrum of this polymer ($M_{n,\text{NMR}} \sim 4400$ g/mol).

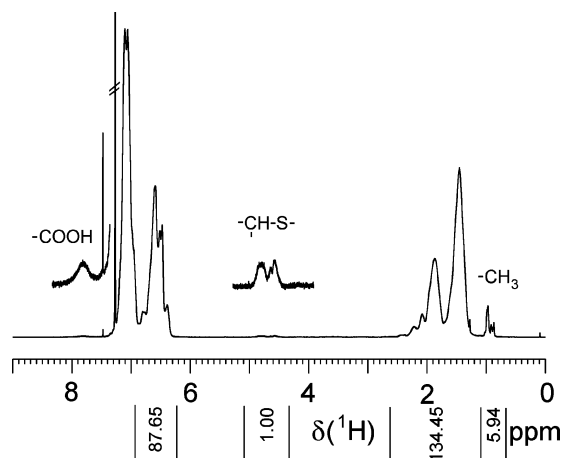


Figure 8. ^1H NMR spectrum of α,ω -carboxylic acid terminated polystyrene synthesized using 2,2'-[carbonothiois(bis(thio))]bis(2-methylpropionic acid) as CTA (solvent: CDCl_3).

The signal groups of methine protons neighboring to the trithiocarbonyl group (4.4–4.9 ppm) and of the methyl protons of the 2-methylpropionic acid end groups (0.8–1.05 ppm) can be well observed. The chemical shift of the methyl protons corresponds with a 2-methylpropionic acid group bonded to the PS chain but not with a trithiocarbonyl group (~ 1.7 ppm from CTA data). Considering the SCH:CH₃ intensity ratio of $\sim 1:6$, a nearly perfect α,ω -termination by 2-methylpropionic acid groups bonded to PS can be concluded. This is also confirmed by the ^{13}C NMR spectrum (Figure SI 4). Based on the ^{13}C NMR data of the CTA, the carboxyl signal of a 2-methylpropionic acid group bonded to trithiocarbonyl is expected at ~ 180 ppm. Only a very weak signal at 179.3 ppm can be identified by 2D NMR (Figure SI 5) whereas an intense signal at 183.4 ppm represents the 2-methylpropionic acid group bonded to PS. This model RAFT polymerization suggests that this CTA results in well-defined PS bearing a trithiocarbonyl group in the backbone and two carboxylic acid groups as α,ω -termination. This is in accordance with the polymerization of *n*-butyl acrylate using the same CTA.³⁴

The morphology of the functionalized PS particles prepared by RAFT mediated MEP was investigated by SEM (Figure SI 6). Nice spherical particles were observed associated with apparently narrow particle size distribution. The DLS analysis

of the dispersion from RAFT mediated MEP also indicates a narrow particle size distribution (see Table 3).

In order to synthesize the PMC nanoparticles by RAFT mediated MEP and to compare the results with the non-RAFT system that was discussed earlier, we used feed MNP concentration of 8 wt % with respect to monomer. The influence of initiator to CTA mole ratio on the content of MNP in the final composites along with the morphology was investigated in detail. The TGA investigation of the PMC nanoparticles obtained from RAFT mediated MEP showed an enhancement in the MNP content with increasing the amount of CTA in the recipe (Table 4). A high value of 27 wt % of MNP content (PMC 7) in a stable latex could be achieved from a feed MNP concentration of 8 wt %. Comparing the TGA values of the samples prepared by non-RAFT MEP (Table 2), it was quite amazing to reach such a high value of MNP content. The colloidal stability was also an important factor for such particles with high MNP content. An observation of the diluted latex of PMC 6 confirmed a reasonable stability of the latex as it remained stable even after 1 week of standing. Figure 9 shows a comparative stability difference between PMC 2 and

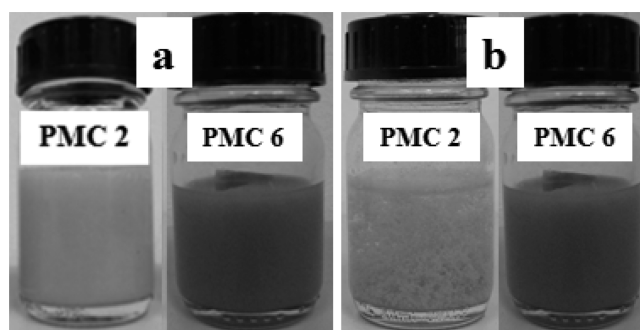


Figure 9. Stability of the diluted latex of PMC nanoparticle dispersion (8 wt % feed MNP content) synthesized by non-RAFT (PMC 2) and RAFT mediated (PMC 6) MEP. (a) Immediately and (b) 1 week after polymerization.

PMC 6. The DLS analysis of all PMC nanoparticles prepared in this study also suggests a reasonably good distribution of the particle size (Table 4).

Apart from this, the MNP content of the final composite could also be controlled from a constant feed amount just by varying the monomer conversion, as shown in Table 4 in the case of PMC 6. We continued the polymerization of PMC 6 up to 40 h to achieve maximum possible conversion in the given recipe. The conversion of monomer increased with the time of polymerization, as expected for a typical RAFT polymerization,

Table 4. Characterization Results for PMC Nanoparticles Synthesized by RAFT Mediated IL Stabilized MEP

sample ^a	polymerization time (h)	AIBN:CTA (mole ratio)	av particle size (nm) [dispersion index]	coagulum (wt %)	SC (wt %)	monomer conv (%)	MNP content from TGA (wt %)
PMC 5	14	1:1	182 [0.09]	3	13	60	13.4
PMC 6 (14)	14	1:2	224 [0.12]	0	11	52	19.2
PMC 6 (22)	22	1:2	222 [0.17]	2	13	64	11.1
PMC 6 (40)	40	1:2	216 [0.22]	7	15	74	8.9
PMC 7	14	1:4	242 [0.29]	0	7	34	27.3
PMC 8	20	3:1	206 [0.10]	4	15	75	6.8
PMC 9 ^b	20	3:1	210 [0.12]	6	15	74	7.0

^aIn all experiments, feed MNP concentration was 8 wt % with respect to styrene, and IL 1 was used as surfactant (exception PMC 9). ^bIL 2 was used as surfactant.

which finally led to a decrease in the final content of MNP since it approached the feed value. Thus, the MNP content in the resulting PMC, starting from 8 wt % in the feed, varied from 19.2 to 8.9 wt % depending on the monomer conversion. To investigate the influence of AIBN to CTA mole ratio on the final MNP content of PMC as well as on the outcome of the polymerization, a series of experiments were performed by changing AIBN to CTA mole ratio but keeping the MNP content in the feed at 8 wt %. Sample PMC 6 and PMC 7 were absolutely free of coagulum whereas the others ended up producing low amount of coagulum. With increase in the amount of AIBN, or better lowering the CTA content in comparison to AIBN, the coagulum started to appear, reaching a large amount associated with the reduction of MNP content in the final PMC nanoparticles (PMC 8). A similar trend was also observed in case of IL2 stabilized RAFT mediated MEP (PMC 9).

In order to explain the production of PMC with a higher final MNP content than the initial feed amount, we took in account the solid content (SC) of each experiment and the monomer conversion calculated from SC. The value of SC and corresponding monomer conversion value is shown in Table 4. With the increase in concentration of CTA, the SC as well as the conversion was reduced. This was in accordance with the expectation as the CTA is able to control the rate of polymerization and thus, with increasing the amount of CTA while keeping the amount of AIBN constant at fixed polymerization conditions, one should obtain a lower conversion of monomer. The residual monomer that remained in the droplets evaporated out during the vacuum drying leaving the organic content of the material much lower compared to the theoretical one. Hence, the TGA investigation of the PMC nanoparticles prepared by RAFT mediated MEP always revealed a higher content of MNP compared to the theoretically predicted one. In case of non-RAFT MEP (Table 2), the monomer conversion was above 90% (PMC 2 and PMC 4) accompanied by a loss of MNP via the formation of coagulum. Thus, the final content of MNP could never reach even near the theoretical value. As discussed before, in case of PMC 6, different MNP content was possible to achieve in a single experiment just by controlling the time of polymerization. This is quite in accordance with the fact that with increasing the polymerization time, following the typical RAFT kinetics, the monomer conversion also increases, consequently the amount of residual styrene that evaporates during the drying process is reduced and as a result of that the organic and inorganic content of the material approaches the feed composition.

Investigation of Morphology Using TEM Analysis. In order to make a correlation between the above results and the morphological characteristics of the PMC nanoparticles, TEM investigations were performed with the samples containing similar feed MNP content of 8 wt %. It is clear from the images of the samples PMC 2 and PMC 4 that in both cases the MNP were not homogeneously distributed over all PS particles. A large number of pure PS nanoparticles were observed beside the PMC nanoparticles (Figure 10a,c). The reason for the existence of pure PS particles was not, or not only, the micellar nucleation that might happen in the case of IL 1 stabilized MEP; otherwise, we would not observe the presence of such particles in the IL 2 stabilized MEP where the concentration of IL 2 was far below its CMC. It can be speculated that the strong magnetic attraction between the individual MNP restricts them

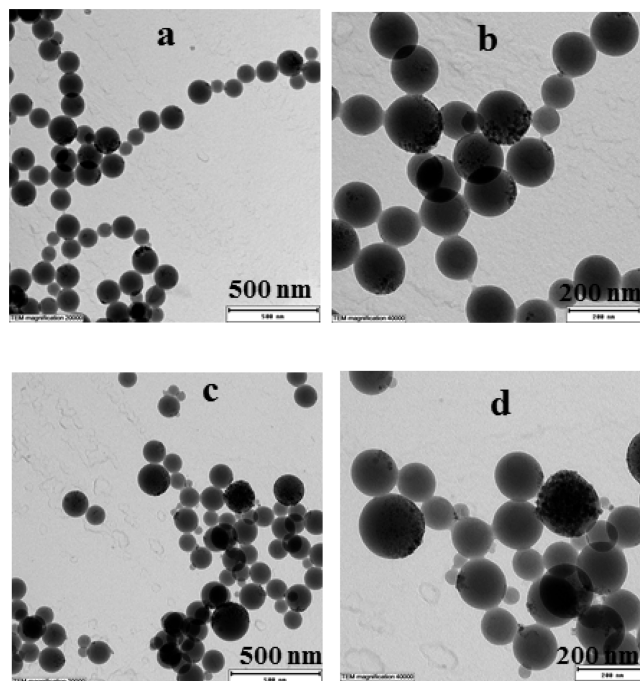


Figure 10. TEM image of the IL stabilized MEP showing inhomogeneous distribution of MNP. (a) and (b) represent the morphology from IL 1 stabilized MEP (PMC 2) at two different magnifications, whereas (c) and (d) represent the same from IL 2 stabilized MEP (PMC 4).

from being distributed all over the PS particles. Also, within the individual composite particles, MNP were not delocalized over the entire particle; rather they were accumulated on some specific areas near the surface of the polymer particle (Figure 10b,d), forming a patchy morphology. Elaissari et al.²² described the reasons for the surface localization and agglomeration of OA coated MNP in the PS particles synthesized by MEP. It was explained on the basis of the mechanism of AIBN initiated MEP where the polymerization propagates toward the surface of monomer droplets and as a consequence the MNP were pushed toward the surface of the droplet due to the poor compatibility between PS matrix and coated OA layer on MNP surface, as indicated in Figure 7. As a result, an anisotropic Janus like morphology was developed.

Beside the above morphology, some other areas of the specimen were also investigated in order to explain the relatively broad particle size distribution as well as the formation of coagulum. Eventually, it was observed that in some areas of the specimen with MNP patches the particles showed a tendency toward agglomeration due to MNP attraction which might lead to inefficient stabilization and the formation of coagulum. Furthermore, some particles were found to stick together forming aggregates which may result in a broader particle size distribution (Figure SI 7).

TEM investigations of the samples prepared by RAFT mediated MEP were also performed to explain the large MNP content of the final PMC nanoparticles combined with still a high stability of the latex and to gain information about the distribution of MNP inside the PS particles. From Table 4, it can be observed that the gradual enhancement in the MNP content of PMC nanoparticles is associated with reduction in monomer conversion with increase in the AIBN to CTA mole ratio. Figure 11 depicts TEM image of PMC 6 and PMC 7 with

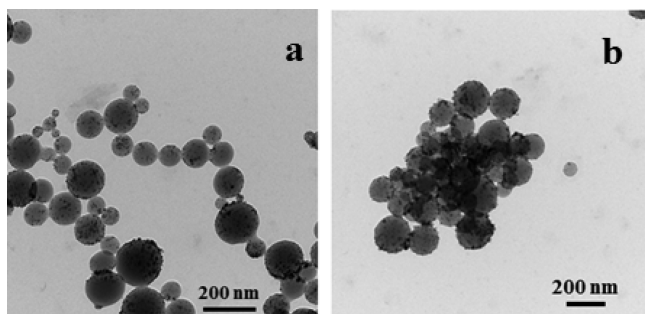


Figure 11. TEM image of the PMC nanoparticles synthesized by RAFT mediated MEP, showing homogeneous distribution of MNP among the PS particles. (a) PMC 6 (14), AIBN to CTA = 1:2; (b) PMC 7, AIBN to CTA = 1:4.

an AIBN to CTA mole ratio of 1:2 and 1:4, respectively. A real homogeneous distribution of MNP was observed among the PS composite particles. Almost no pure PS particles were found which is quite impressive compared to the non-RAFT one (Figure 10a,c). Similar to PMC 2, a significant amount of MNP was found to be attached to the surface of polymer particles which was quite expected as all of the experiments in our study use AIBN initiated polymerization.

To analyze the influence of AIBN to CTA mole ratio on the morphology of PMC nanoparticles, TEM investigation of PMC 8 was performed with a high AIBN content compared to CTA of 3:1 (Figure 12a). The MNP were observed to distribute

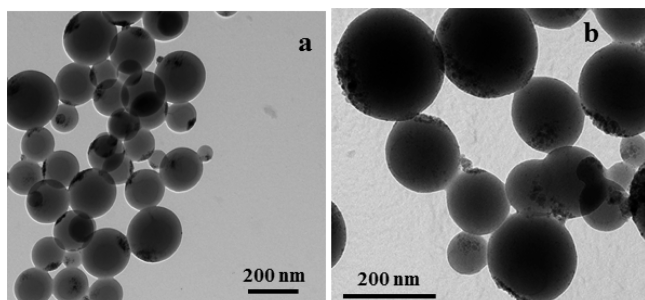


Figure 12. TEM image of (a) PMC 8 and (b) PMC 9 showing anisotropic distribution of MNP (Janus-like morphology) in all PMC nanoparticles.

among all the PS particles as found in case of PMC 6 (Figure 11a). But a striking difference was detected in the location of MNP in the individual PS particles. The MNP were not dispersed homogeneously within the PS particles; rather, they were confined to a specific area on the PS surface nearly similar to that of PMC 2 or PMC 4. But due to the efficiency of CTA regarding the distribution of MNP in all polymer particles (as shown in Figure 11), no existence of pure PS particles was found. Consequently, the anisotropic (Janus-like) location of MNP in the polymer was spread over all the PS particles in the latex. Altering the surfactant to IL 2 (PMC 9) did not influence the morphology as the MNP were nicely distributed in the PS particles (Figure 12b). Thus, a similar anisotropic morphology developed also in this case. One can speculate that with increasing the AIBN content, less PS chains are functionalized with COOH end groups, and thus, a lower number of chains can undergo specific interactions with the MNP.

Hence, the carboxyl terminated CTA proved to be an effective component in the synthesis of PMC nanoparticles.

Besides enhancing the MNP content of the PMC nanoparticles, it could control the morphology as well, depending on the mole ratio of initiator to CTA. The different morphologies that were possible to achieve are schematically outlined in Figure 13.

The morphology I of PMC nanoparticles was observed in several AIBN initiated MEPs and was well explained by Elaissari et al.²² in the SDS stabilized MEP to synthesize anisotropic Janus magnetic polymer particle. But the occurrence of pure polymer particles could not be avoided. On the other hand, a real homogeneous distribution of MNP associated with a nice dispersion of MNP inside the PS particles was observed in morphology II, in which the molar concentration of CTA was higher than that of AIBN. The reason for such morphology was possibly due to the affinity of the surface of MNP toward the carboxylic acid group of CTA attached to the polymer chain end. Lu et al.³³ reported a ligand exchange reaction of OA coated MNP with a carboxyl functionalized CTA in which a partial replacement of OA was described by the CTA. The interaction of CTA with the MNP was mostly through the terminal carboxyl group and the trithio group. In our system, the presence of carboxyl terminated CTA in each of the monomer droplets was proved to be an effective way to distribute the MNP homogeneously between all the styrene droplets which was not possible in the case of the non-RAFT process as shown in Figure 13. During the RAFT polymerization the oligomer PS containing a carboxylic acid and trithiocarbonyl group at their chain possibly interacted with the surface of MNP to disperse them inside each PS droplet, and as a result of that morphology II developed. Because of the complexity of the system under investigation, FTIR analysis could not confirm such interaction of MNP with the carboxyl functionalized PS chain. Another important factor was the low conversion of monomer in RAFT mediated MEP and the resulting lower mass of the PS chains which made the mobility of MNP inside the droplet much easier compared to the non-RAFT MEP and thereby producing a homogeneous dispersion within the PS droplet. Increasing the concentration of AIBN produced a much faster polymerization which led to reasonably higher conversion of monomer (PMC 8 and PMC 9 in Table 4) in a similar reaction time as for PMC 6 or PMC 7. Consequently, the mobility of MNP inside the PS droplet became very low, and accumulation of the nanoparticles at the surface of PS particles due to low compatibility was observed which is represented by morphology III in Figure 13. Attaining the anisotropic Janus morphology in all PMCs reproducibly has been rather a tricky one as a proper optimization of the amount of initiator and CTA needs to be done. Otherwise, a lower concentration of AIBN will lead to morphology II or a higher concentration of AIBN will finally end up producing a high amount of coagulum in the system.

Investigation of Molecular Weight and Dispersity Index. The molecular weight distribution of the PS particles was highly influenced by the presence of MNP in the system. In absence of MNP, IL stabilized free radical MEP led to high molecular weight of PS (e.g., M_n of PS1:2.61 × 10⁶ g/mol) which was expected from a heterogeneous polymerization system, whereas via RAFT MEP lower molecular weights were obtained (e.g., M_n of PS3:1.8 × 10⁴ g/mol, Table 3). In the presence of MNP the M_n value of the product of free radical MEP remained high but the distribution became broader. The dispersity index increased from about 2 to 4–5. The appearance of broader distribution was possible to overcome using RAFT mediated MEP. In all the samples prepared by

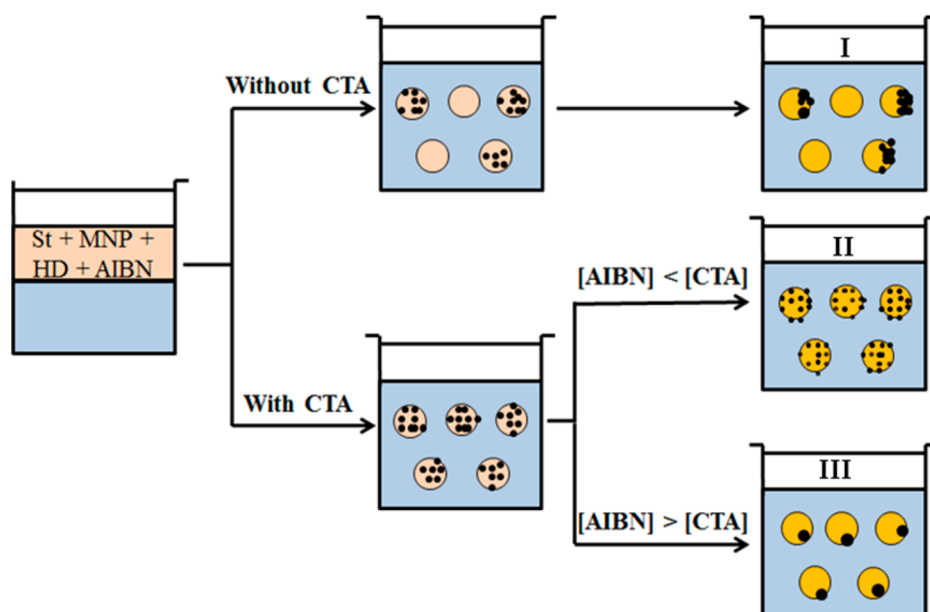


Figure 13. Representation of the different morphologies I–III that are possible to develop through IL stabilized MEP in the absence and presence of CTA.

Table 5. Molecular Weight Distribution of PS in PMC Nanoparticles

sample	feed MNP ^a (wt %)	AIBN (g)	CTA (g)	AIBN:CTA (mole ratio)	conv of monomer (%)	M_n (g/mol)	dispersity index \mathcal{D}
PMC 1	4	0.130			96	2.4×10^5	5.8
PMC 2	8	0.130			90	2.2×10^5	5.1
PMC 3	12	0.130			80	2.0×10^5	4.1
PMC 4 ^b	8	0.130			90	1.2×10^5	4.8
PMC 5	8	0.022	0.038	1:1	60	25000	1.9
PMC 6 (14) ^c	8	0.022	0.076	1:2	52	7000	1.5
PMC 6 (22) ^c	8	0.022	0.076	1:2	64	14000	1.7
PMC 6 (40) ^c	8	0.022	0.076	1:2	74	18000	1.7
PMC 7	8	0.022	0.150	1:4	34	2500	1.5
PMC 8	8	0.130	0.076	3:1	75	20000	1.7
PMC 9 ^b	8	0.130	0.076	3:1	74	20000	1.8

^aIn all experiments, feed MNP concentration was 8 wt % with respect to styrene. ^bIn the case of PMC 4 and PMC 9, IL 2 was used as surfactant. In all other cases, IL 1 was used as surfactant. ^cValues in the parentheses represent the time of polymerization in the synthesis of PMC 6.

RAFT MEP, the dispersity index was reduced down to 1.5. Thus, much better control over the polymerization was possible to achieve. The M_n value could also be controlled by a proper tuning of AIBN to CTA mole ratio and by monomer conversion. In the case of PMC 6, a nearly linear increase in M_n value with time of polymerization and consequently with the increase in the conversion of monomer clearly fits with a controlled radical polymerization system. The slight deviation from the linearity in the development of M_n with respect to time of polymerization (or conversion of monomer) may arise from the influence of MNP within the droplets.

Magnetic Property Investigation. The magnetic properties of the synthesized PMC nanoparticles were investigated using VSM analysis. All the materials showed a typical paramagnetic behavior at the experimental condition (Figure 14). The saturation magnetization (M_s) of the samples was in accordance with the MNP content value. The morphological divergence did not show any significant difference in the M_s values. Among the PMC nanoparticles synthesized in this study, PMC 7 displayed the highest value of M_s (16.60 emu/g) as expected from its high MNP content composition. The magnetization curve clearly indicates that it is possible to

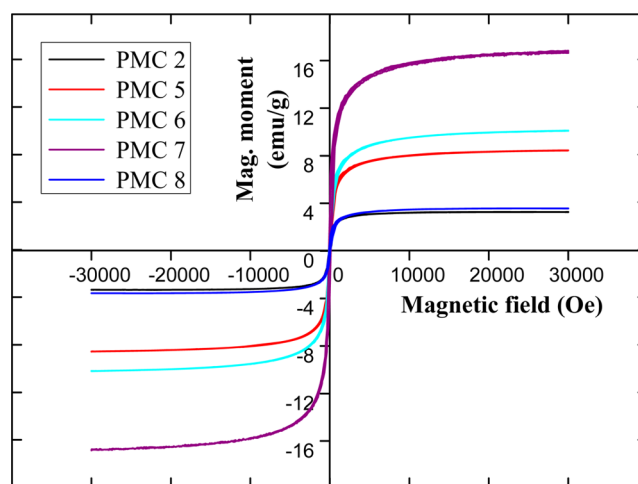


Figure 14. Magnetization curve of PMC nanoparticles with different MNP content which were synthesized by IL 1 stabilized MEP.

control the M_s value by tuning the MNP content of the PMC nanoparticles through RAFT mediated MEP. From the similar

feed MNP content, a different range of M_n could be achieved. This provides a big advantage in the application purpose of the magnetic materials where the extent of magnetization holds a vital key for the outcome of the experiment.

CONCLUSION

In this work we could successfully perform MEP of styrene using imidazole based ILs as surfactants. Furthermore, molecular weight and dispersity index of the polymer could be controlled by employing RAFT mediated IL stabilized MEP. Because of the availability of CTA with different functional groups, one can obtain several kinds of internally functionalized polymer particles through this approach. On the other hand, the presence of IL at the surface of polymer particles can be easily utilized through the ion exchange capability of IL that can offer the possibility of dispersing the same polymer particle in different solvents ranging from polar to nonpolar in nature.

Magnetic polymer particles were synthesized using IL stabilized MEP employing first a free radical process, but high content of MNP in the composite particles could not be achieved due to increasing instability in the dispersion with increasing MNP in the feed associated with the formation of a high amount of coagulum. This problem was overcome using RAFT mediated IL stabilized MEP. Different MNP contents ranging from 8 to 27 wt % could be reached from 8 wt % feed concentration, depending on the final monomer conversion, with good to moderate colloidal stability. Considering the advantages of a single step miniemulsion process, the RAFT miniemulsion approach proved to be a promising method to enhance the final MNP content in the composites. On the other hand, different morphologies could be developed by tuning the initiator to CTA mole ratio, but fully avoiding the preparation of polystyrene particles lacking any MNP due to the improved interactions of the MNP with carboxylic acid end groups of the polystyrene chains prepared with the RAFT mechanism. Combining several characterization techniques, the colloidal stability, morphology, structural elucidation, and composition of the materials were confirmed. As RAFT chemistry employed here is quite compatible with the biological system, a biocompatible monomer can well be utilized according to this approach to prepare magnetic biocompatible polymer nanoparticles for suitable biomedical applications. Beside the above benefits of RAFT mediated MEP approach for synthesizing PMC nanoparticles, a major drawback lies in the low conversion of monomer in case of experiments consisting of high feed MNP concentration which may restrict this method in several applications, even though it has been shown that this can be overcome by increasing the polymerization time. Therefore, at present, we are further improving the formation of PMC nanoparticles through the RAFT mediated MEP approach.

ASSOCIATED CONTENT

Supporting Information

NMR spectra of ILs, CTA and carboxyl functionalized PS, comparative dispersion analysis of OA coated MNP in water and toluene, SEM image of PS 3, TEM image of OA coated MNP sticky particles of PMC 2, SEM images of PS nanoparticles prepared by SDS/CTAB stabilized MEP and comparative study between IL, SDS and CTAB regarding the influence of surfactant to monomer ratio on average particle size of polystyrene. This material is available free of charge via the Internet at <http://pubs.acs.org>.

AUTHOR INFORMATION

Corresponding Author

*E-mail voit@ipfdd.de (B.V.).

Notes

The authors declare no competing financial interest.

ACKNOWLEDGMENTS

The authors acknowledge Petr Fomanek and Uta Reuter for TEM, Maria Auf der Landwehr for SEM, Kerstin Arnhold for TGA, and Petra Treppe for GPC analysis. We have been grateful to Dr. Volker Neu of IFW Dresden (Germany) for providing the VSM instrument for magnetic property measurement. S. Chakraborty thanks Dr. Jürgen Pionteck for important advice in this work.

REFERENCES

- (1) Cheng, F.-Y.; Su, C.-H.; Yang, Y.-S.; Yeh, C.-S.; Tsai, C.-Y.; Wu, C.-L.; Wu, M.-T.; Shieh, D.-B. *Biomaterials* **2005**, *26*, 729–738.
- (2) Elaissari, A.; Rodrigue, M.; Meunier, F.; Herve, C. *J. Magn. Magn. Mater.* **2001**, *225*, 127–133.
- (3) Akgöl, S.; Kaçar, Y.; Denizli, A.; Arica, M. Y. *Food Chem.* **2001**, *74* (3), 281–288.
- (4) Gupta, P. K.; Hung, C. T. *Life Sci.* **1989**, *44*, 175–186.
- (5) Langer, R. *Science* **1990**, *249*, 1527–1533.
- (6) Hancock, J. P.; Kemshead, J. T. *J. Immunol. Methods* **1993**, *164*, 51–60.
- (7) Yang, S.-M.; Kim, S.-H.; Lim, J.-M.; Yi, G.-R. *J. Mater. Chem.* **2008**, *18*, 2177–2190.
- (8) Yoon, J.; Lee, K. J.; Lahann, J. *J. Mater. Chem.* **2011**, *21*, 8502–8510.
- (9) Ahmadi, A.; Williamson, B. H.; Theis, T. L.; Powers, S. E. *J. Cleaner Prod.* **2003**, *11*, 573–582.
- (10) Ding, S.; Xing, Y.; Radosz, M.; Shen, Y. *Macromolecules* **2006**, *39*, 6399–6405.
- (11) Yuet, K. P.; Hwang, D. K.; Haghgooeie, R.; Doyle, P. S. *Langmuir* **2009**, *26*, 4281–4287.
- (12) Lattuada, M.; Hatton, T. A. *J. Am. Chem. Soc.* **2007**, *129*, 12878–12889.
- (13) Braconnot, S.; Eissa, M. M.; Elaissari, A. *Colloid Polym. Sci.* **2013**, *291*, 193–203.
- (14) Chen, K.; Zhu, Y.; Zhang, Y.; Li, L.; Lu, Y.; Guo, X. *Macromolecules* **2011**, *44*, 632–639.
- (15) Ramírez, L. P.; Landfester, K. *Macromol. Chem. Phys.* **2003**, *204*, 22–31.
- (16) Chen, Z.; Peng, K.; Mi, Y. *J. Appl. Polym. Sci.* **2007**, *103*, 3660–3666.
- (17) Luo, Y.-D.; Dai, C.-A.; Chiu, W.-Y. *J. Polym. Sci., Part A: Polym. Chem.* **2008**, *46*, 1014–1024.
- (18) Mahdavian, A. R.; Ashjari, M.; Mobarakeh, H. S. *J. Appl. Polym. Sci.* **2008**, *110*, 1242–1249.
- (19) Qian, Z.; Zhang, Z.; Chen, Y. *J. Colloid Interface Sci.* **2008**, *327*, 354–361.
- (20) Ramos, J.; Forcada, J. *Langmuir* **2011**, *27*, 7222–7230.
- (21) Mori, Y.; Kawaguchi, H. *Colloids Surf., B* **2007**, *56*, 246–254.
- (22) Kaewsaneha, C.; Tangboriboonrat, P.; Polpanich, D.; Eissa, M.; Elaissari, A. *J. Polym. Sci., Part A: Polym. Chem.* **2013**, *51*, 4779–4785.
- (23) Lu, S.; Ramos, J.; Forcada, J. *Langmuir* **2007**, *23*, 12893–12900.
- (24) Vanyür, R.; Biczók, L.; Miskolczy, Z. *Colloids Surf., A* **2007**, *299*, 256–261.
- (25) Guerrero-Sanchez, C.; Erdmenger, T.; Šereda, P.; Wouters, D.; Schubert, U. S. *Chem.—Eur. J.* **2006**, *12*, 9036–9045.
- (26) Yan, F.; Texter, J. *Chem. Commun.* **2006**, 2696–2698.
- (27) Costa, C.; Santos, V. H. S.; Dariva, C.; Santos, A. F.; Fortuny, M.; Araujo, P. H. H.; Sayer, C. *J. Appl. Polym. Sci.* **2013**, *127*, 448–455.
- (28) Huang, X.; Sudol, E. D.; Dimonie, V. L.; Anderson, C. D.; El-Aasser, M. S. *Macromolecules* **2006**, *39*, 6944–6950.

- (29) de Brouwer, H.; Tsavalas, J. G.; Schork, F. J. *Macromolecules* **2000**, *33*, 9239–9246.
- (30) Dong, S.; Cheng, S.; Zetterlund, P. B. *J. Polym. Sci., Part A: Polym. Chem.* **2013**, *51*, 2104–2109.
- (31) Lai, J. T.; Filla, D.; Shea, R. *Macromolecules* **2002**, *35*, 6754–6756.
- (32) Zhang, Q.; Yang, F.; Tang, F.; Zeng, K.; Wu, K.; Cai, Q.; Yao, S. *Analyst* **2010**, *135*, 2426–2433.
- (33) Bechthold, N.; Tiarks, F.; Willert, M.; Landfester, K.; Antonietti, M. *Macromol. Symp.* **2000**, *151*, 549–555.
- (34) Jiang, X.; Schoenmakers, P. J.; Lou, X.; Lima, V.; van Dongen, J. L. J.; Brokken-Zijp, J. *J. Chromatogr. A* **2004**, *1055*, 123–133.
- (35) Xiao, Z.-P.; Yang, K.-M.; Liang, H.; Lu, J. *J. Polym. Sci., Part A: Polym. Chem.* **2010**, *48*, 542–550.